Available online at www.sciencedirect.com

SCIENCE DIRECT®

ACADEMIC PRESS

Journal of Molecular Spectroscopy 217 (2003) 222–238

Journal of MOLECULAR SPECTROSCOPY

www.elsevier.com/locate/jms

The absorption spectrum of H_2S between 9540 and 10 000 cm^{-1} by intracavity laser absorption spectroscopy with a vertical external cavity surface emitting laser☆

Yun Ding,[a,b] Olga Naumenko,[c] Shui-Ming Hu,[b] Qingshi Zhu,[b] Elena Bertseva,[a] and Alain Campargue[a,*]

[a] *Laboratoire de Spectrométrie Physique (associated with CNRS, UMR C5588), Université Joseph Fourier de Grenoble, B.P. 87, 38402 Saint-Martin-d'Hères Cedex, France*

[b] *Open Research Laboratory of Bond-Selective Chemistry, University of Science and Technology of China, Hefei 230026, PR China*

[c] *Institute of Atmospheric Optics, SB, Russian Academy of Science, Tomsk, Russia*

Received 17 July 2002; in revised form 2 October 2002

Dedicated to Professor H. Bürger on the occasion of his 65th birthday.

Abstract

An Intracavity Laser Absorption Spectrometer (ICLAS) based on a Vertical External Cavity Surface Emitting Laser (VECSEL) has been used to record the absorption spectrum of H_2S between 9540 and 10 000 cm^{-1} with pressures up to 122 Torr (160.5 hPa) and equivalent absorption path lengths up to 45 km. More than 1600 absorption lines were attributed to the transitions reaching the highly excited $(40^{\pm}, 0)$, $(30^{\pm}, 2)$, and $(11^{+}, 4)$ states (local mode notation). The existing information relative to the $(40^{\pm}, 0)$ local mode bright pair at 9911.02 cm^{-1} was considerably enlarged, while the other states are reported for the first time. Eight hundred and ninety two precise energy levels were derived, including 181 and 28 levels for the $H_2{}^{34}S$ and $H_2{}^{33}S$ minor isotopomers, respectively. These energy levels were fitted using a Watson-type rotational Hamiltonian and the spectroscopic parameters were obtained, yielding an rms deviation of 0.006 cm^{-1} for the $H_2{}^{32}S$ species—close to the experimental accuracy. The dark states—$(20^{+}, 4)$ and $(11^{+}, 4)$—at 9647.77 and 9744.88 cm^{-1}, respectively, were found to perturb the observed energy levels and were then included into the final energy levels modeling. The $(40^{\pm}, 0)$ states are very close to the local mode limit, i.e., with a mostly identical rotational structure. The $(30^{\pm}, 2)$ states are separated by 0.077 cm^{-1} and this separation holds for most of the rotational sublevels. The resonance interactions between the three local mode pairs—$(40^{\pm}, 0)$, $(30^{\pm}, 2)$, and $(20^{\pm}, 4)$—and the $(11^{+}, 4)$ state affect in some cases specifically one of the component of the pair and then the energy separation of the corresponding near degenerate rotational levels. Line intensities were obtained on the basis of the relative intensities measured by ICLAS and from absolute values of the stronger lines measured separately by Fourier Transform Spectroscopy associated with a multipass cell. The transition intensities could be successfully modeled and the integrated band intensities are given and discussed.

1. Introduction

Intracavity Laser Absorption Spectroscopy (ICLAS) is a highly sensitive absorption technique which has been extensively applied above 10 000 cm^{-1} with Ti:sapphire and dye lasers. An interesting development towards the near infrared region has been recently achieved in Grenoble by using Quantum Wells semiconductor structures as amplification media. After the first developments and the study of the dynamics of the Vertical External Cavity Surface Emitting Lasers (VECSEL) by Garnache et al. [1,2], ICLAS-VECSELs were used between 9400 and 10 100 cm^{-1} for the overtone spectroscopy of propyne [3], N_2O [4], and CO_2 [5]. The present study is devoted to the absorption spectrum of hydrogen sulfide between 9500 and 10 000 cm^{-1}.

☆ Supplementary data for this article are available on ScienceDirect.

* Corresponding author. Fax: +4-76-51-45-44.
E-mail address: alain.CAMPARGUE@ujf-grenoble.fr (A. Campargue).

0022-2852/03/$ - see front matter © 2003 Elsevier Science (USA). All rights reserved.
doi:10.1016/S0022-2852(02)00037-1

We have extensively studied the overtone spectrum of H_2S by ICLAS with Ti:sapphire and dyes above 10 000 cm^{-1} [6–10]. Our last report was, for instance, devoted to the highest overtone transition of H_2S reported so far, observed in the 16 180–16 440 cm^{-1} region and corresponding to an excitation of the $(70^{\pm}, 0)$ local mode pair [10]. The present investigation concerns the spectral region between 9540 and 10 000 cm^{-1} involving mainly the $(40^{\pm}, 0)$ local mode pair near 9911 cm^{-1}. This spectral region was not previously investigated by any high sensitive laser technique and the existing information relative to the $(40^{\pm}, 0)$ local mode pair was retrieved from Fourier Transform spectra recorded at Kitt Peak with a multipass cell with optical path lengths up to 433 m [11]. The increased sensitivity presently achieved has allowed to extend considerably the knowledge of the rotational structure of the $(40^{\pm}, 0)$ local mode pair, while three states involving bending excitation could be newly detected from weak transitions.

2. Experiment

We used the experimental set-up based on a VECSEL configuration similar to that developed in [2] and described in [4]. The tuning of the wavelength is obtained by translating the sample position and varying the temperature between −30 and +60 °C. The typical temperature tuning rate is 0.5 cm^{-1}/°C. The pump laser is a commercial diode lasing at 830 nm and the threshold power of the VECSEL was about 100 mW. The pump was driven by a pulsed voltage. After the generation time, the output beam was deflected by an acousto-optic modulator into the grating spectrograph equipped with a 3724-pixels silicon array in its focal plane (see [4] for more details). The spectral region simultaneously recorded with a typical spectral resolution of 0.03 cm^{-1} was about 12 cm^{-1} within a few seconds. Generation times ranging between 200 and 400 μs corresponding to equivalent absorption path lengths of 30–60 km were adopted leading to a typical sensitivity of $\alpha \approx 10^{-9}$ cm^{-1}. The wavenumber calibration procedure of the spectra requires two reference lines for each spectrograph position. In the high energy part of the considered spectral range, atmospheric water lines [12] could be used as reference. However, in the lower energy part, the water lines are too sparse and weak. For this purpose, the Fourier Transform Spectrum of H_2S was recorded in Hefei by using a Bruker 120 HR interferometer associated with a multipass cell to use some relatively strong absorption H_2S lines to calibrate the numerous supplementary weaker lines observed by ICLAS. A tungsten source, near-IR quartz beam splitter and a Ge detector were used. The unapodized resolution was 0.02 cm^{-1} (1/maximum optical path difference). Scans (1150) were accumulated to improve the signal-to-noise ratio. The sample pressure and the absorption path length were $P = 206$ hPa and $l = 87$ m, respectively, leading to $P \times l$ value close to that of [11]. In term of sensitivity, the signal-to-noise ratio presently achieved is slightly larger than that of [11]. The calibration of the FT spectrum was performed with H_2O lines taken from [12] leading to

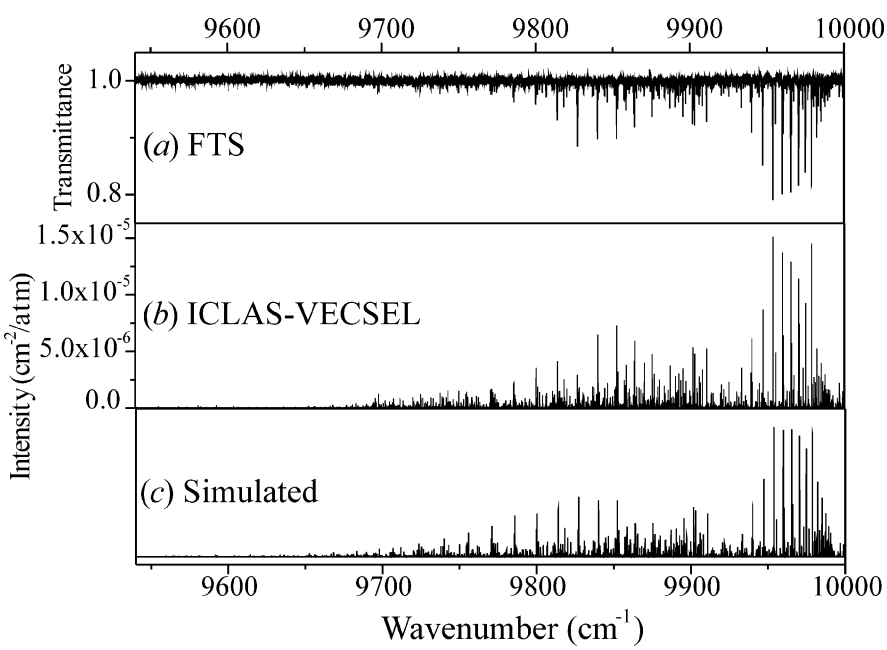

Fig. 1. Overview of the absorption spectrum of H_2S between 9540 and 10 000 cm^{-1}. (a) FT spectrum used to calibrate ICLAS (resolution 0.02 cm^{-1}, pressure 206 hPa, absorption path length 87 m). (b) Experimental ICLAS-VECSEL stick spectrum recorded with an equivalent absorption path length 30 km and a pressure 35.5 hPa (27 Torr). The absolute values of the line intensities were deduced from the FT spectrum. (c) Simulated spectrum of H_2S. The line positions were calculated using the Hamiltonian parameters of Table 4.

an excellent agreement with the values obtained in [11]. From the comparison of the wavenumber values obtained by using independent reference lines, we estimate the absolute wavenumber accuracy of the ICLAS line positions to be better than $0.01\,\mathrm{cm}^{-1}$.

An overview of the FT and ICLAS spectra are presented in Fig. 1 while a comparison for two specific spectral regions is displayed in Figs. 2 and 3.

3. Rovibrational analysis

Among the 1630 absorption lines measured between 9541 and $10\,001\,\mathrm{cm}^{-1}$, about 1300 were assigned to the $H_2{}^{32}S$ species. The line list is attached to the present paper as Supplementary Material. The spectrum is dominated by transitions reaching the (3 0 1) and (2 0 2) pure stretching vibrational states (in normal mode (NM)

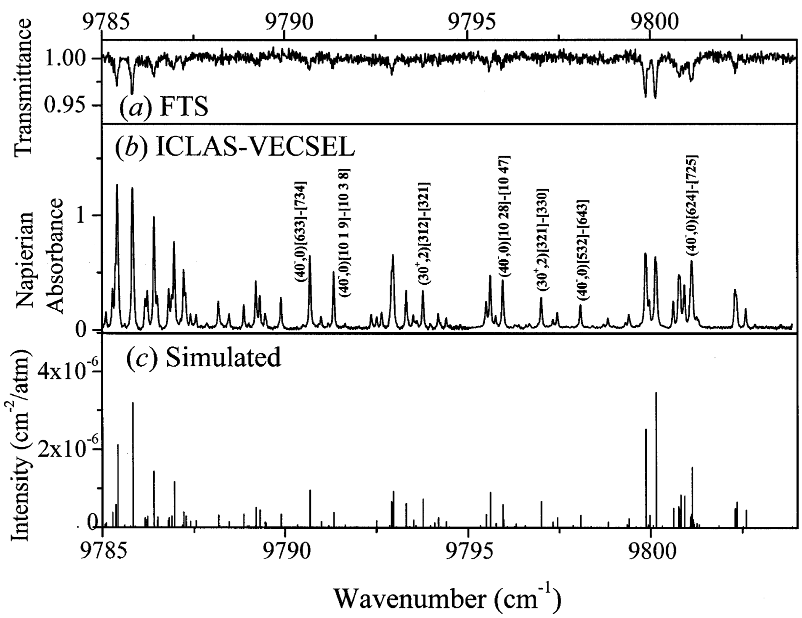

Fig. 2. The absorption spectrum of H_2S between 9785 and $9804\,\mathrm{cm}^{-1}$. (a) FT spectrum used to calibrate ICLAS (resolution $0.02\,\mathrm{cm}^{-1}$, pressure 206 hPa, absorption path length 87 m). (b) Experimental ICLAS-VECSEL spectrum recorded with an equivalent absorption path lengths 30 km, pressure 35.5 hPa (27 Torr). (c) Simulated spectrum of H_2S. The line positions were calculated using the Hamiltonian parameters of Table 4.

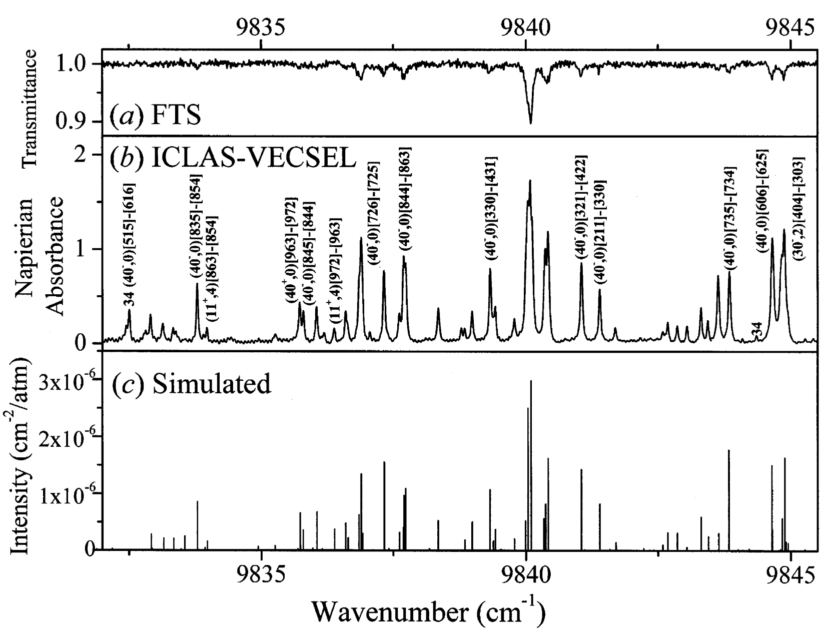

Fig. 3. Same as Fig. 2 for the $9832–9846\,\mathrm{cm}^{-1}$ region. Note that the lines due to the $H_2{}^{34}S$ minor isotope, marked “34,” were not considered in the simulated spectrum.

notation) which form the $(40^{\pm},0)$ local mode (LM) pair at 9911.023 cm^{-1}. Compared to the previous FT study of [11], the higher sensitivity presently achieved has allowed increasing considerably the number of rotational levels. Interestingly, three weaker bands corresponding to the (2 2 1) and (1 2 2) vibrational levels ($(30^{\pm},2)$ in LM notation) and the highly excited bending level (1 4 1) ($(20^{-},4)$ in LM notation) could be detected for the first time. The vibrational term values of the states under consideration are gathered in Table 1 together with their NM and LM labelings and the number of levels derived for each state.

Since a significant number of the analyzed transitions are weak single lines not included into Ground State Combination Difference (GSCD) relations, the assignment process relied greatly on the predictive calculations based on the rotational, centrifugal distortion, resonance, and transition moment parameters which were obtained and permanently refined by fitting the experimental energy levels and line intensities (see below). As a result of the spectrum assignment, 892 precise energy levels were derived for the three $H_2{}^{32}S$, $H_2{}^{33}S$, and $H_2{}^{34}S$ isotopomers by adding the ground state energies [13] to the identified transitions. The experimental accuracy calculated from the levels observed through several transitions is 0.003 cm^{-1}. In contrast to the approach adopted in [9] where the same set of energy levels was derived for the $(40^{\pm},1)$ states by treating simultaneously, in the C_s symmetry group, the corresponding A and B transitions of the $(40^{\pm},1)$—(0 0 0) band, in this study, we derived separate energy level sets for each component of the $(40^{\pm},0)$ LM pair. The reason for this choice is the observation of a systematic shift of 0.005–0.010 cm^{-1} between the two sets of energy levels (the levels of the $(40^{+},0)$ state being slightly lower than those of the $(40^{-},0)$ state). This shift increases up to 0.025 cm^{-1} for high values of the rotational quantum number J. In addition, resonance interactions with the other considered vibrational states affect differently a number of levels of the $(40^{\pm},0)$ pair and increase the separation up to 0.076 cm^{-1}. As a result, 178 and 157 of the identified levels (compared to 73 and 47, respectively, in [11]) were assigned to the $(40^{+},0)$ and $(40^{-},0)$ $H_2{}^{32}S$ local mode states, respectively, while 133, 122, 91, and 2 were attributed to the $(30^{-},2)$, $(30^{+},2)$, $(20^{-},4)$, and $(11^{+},4)$ $H_2{}^{32}S$ states, respectively. These observed energy levels followed by experimental uncertainties, number of lines used for the energy level determination, and deviations from the calculated values (see below) are listed in Table 2 for the $(40^{\pm},0)$ local mode pair and in Table 3 for the four other $H_2{}^{32}S$ states. A few energy levels marked by asterisk were found perturbed by dark states not included into our model and then excluded from the fit described hereafter.

Finally 654 of the 683 observed energy levels of $H_2{}^{32}S$ could be reproduced by a Watson-type effective Hamiltonian in I^r representation used for vibrationally diagonal blocks. The resonance Fermi and Coriolis-type operators were taken of the following form:

$$H^F = F_k J_z^2 + F_j J^2 + F_{xy} J_{xy}^2 + \cdots, \quad (1)$$

Table 1
Vibrational assignments, vibrational term values (in cm^{-1}) and band intensities of the different levels of hydrogen sulfide studied between 9540 and 10 000 cm^{-1}

Vibrational state		N^c	E_v			Band intensity ($\times 10^{-4}$ cm^{-2} atm^{-1})	
NM[a]	LM[b]		Obs.	Obs. − Calc. [4]	Obs. − Calc. [16]	Measured	Ref. [15]
$H_2{}^{32}S$							
1 4 1	$20^-,4$	91	9647.167	0.35	0.23	0.142	0.10
0 4 2	$20^+,4$	0	9647.774[d]	0.53	0.11	0.001	0.002
2 4 0	$11^+,4$	2	9744.888[d]	−0.89	−0.92	0.002	0.001
2 2 1	$30^-,2$	133	9806.667	0.21	0.01	0.879	0.01
1 2 2	$30^+,2$	122	9806.733	0.16	−0.07	0.382	3.76
3 0 1	$40^-,0$	178	9911.023	−0.02	0.00	4.84	8.10
2 0 2	$40^+,0$	157	9911.023	−0.04	0.00	1.31	0.15
$H_2{}^{33}S$							
3 0 1	$40^-,0$	17	9907.050[d]		0.01		
2 0 2	$40^+,0$	11	9907.050[d]		0.01		
$H_2{}^{34}S$							
2 2 1	$30^-,2$	34	9798.741[d]		0.02		
1 2 2	$30^+,2$	14	9798.796[d]		−0.06		
3 0 1	$40^-,0$	81	9903.323		0.01		
2 0 2	$40^+,0$	52	9903.313[d]		0.00		

[a] Normal mode labeling.
[b] Local mode labeling.
[c] Number of observed levels.
[d] Effective value (see the text).

Table 2
Rotational energy levels (cm^{-1}) of the $(40^-,0)$ and $(40^+,0)$ vibrational states of $H_2{}^{32}S$ ((3 0 1) and (2 0 2), respectively, in normal mode notation)

J	K_a	K_c	$(40^-,0)$				$(40^+,0)$			
			E_{obs}	σ	N	Δ	E_{obs}	σ	N	Δ
0	0	0	9911.023		1	−0.001	9911.023		1	0.004
1	0	1	9923.861	1	2	0.005	9923.848		1	−0.005
1	1	1	9925.369	1	2	−0.001	9925.365		1	−0.002
1	1	0	9929.253	1	2	0.001	9929.248	2	2	0.001
2	0	2	9946.782	1	3	−0.002	9946.782	4	2	−0.002
2	1	2	9947.148	7	3	0.001	9947.145	3	4	−0.001
2	1	1	9958.781	2	4	−0.002	9958.771		1	−0.009
2	2	1	9963.321	1	2	0.000	9963.315	1	2	−0.004
2	2	0	9966.048	1	3	0.001	9966.038	2	2	−0.005
3	0	3	9978.420	2	2	−0.001	9978.417	3	2	−0.002
3	1	3	9978.362	1	4	−0.003	9978.359	2	2	−0.003
3	1	2	10000.085	2	3	0.001	10000.079	1	2	−0.004
3	2	2	10001.776	2	4	0.000	10001.771	1	4	−0.004
3	2	1	10011.380	1	4	0.001	10011.378	9	2	0.002
3	3	1	10020.386	1	3	0.002	10020.379	2	2	−0.002
3	3	0	10021.960	1	2	−0.004	10021.960	3	3	0.000
4	0	4	10018.758	1	3	0.001	10018.753		1	0.004
4	1	4	10018.752	2	4	−0.001	10018.752		1	0.007
4	1	3	10050.636	2	5	0.001	10050.632	3	3	0.000
4	2	3	10050.250		1	−0.004	10050.246	3	3	−0.006
4	2	2	10070.299	2	4	−0.004	10070.298	2	3	−0.005
4	3	2	10074.776	2	3	−0.006	10074.781	1	4	−0.001
4	3	1	10081.965	1	5	0.000	10081.974	1	2	0.011
4	4	1	10096.654	2	3	0.001	10096.643	3	3	−0.007
4	4	0	10097.431	2	3	0.000	10097.423	1	2	−0.004
5	0	5	10068.041	3	3	−0.001	10068.040		1	0.002
5	1	5	10068.041	1	3	0.000	10068.040		1	0.003
5	1	4	10108.908	2	3	0.005	10108.894	1	2	−0.005
5	2	4	10108.835	2	4	0.002	10108.825		1	−0.001
5	2	3	10140.683	7	4	0.004	10140.678	9	5	0.001
5	3	3	10139.266	1	5	−0.002	10139.259	2	3	−0.008
5	3	2	10157.452	6	3	0.000	10157.446	3	4	−0.005
5	4	2	10166.293	1	4	−0.001	10166.295	5	4	0.002
5	4	1	10171.039	3	4	−0.004	10171.035	1	2	−0.005
5	5	1	10192.175	1	2	0.000	10192.169	3	4	−0.003
5	5	0	10192.515	2	2	0.001	10192.506	4	3	−0.006
6	0	6	10126.250	1	4	0.005	10126.249		1	0.010
6	1	6	10126.248	3	3	0.003	10126.249	1	2	0.010
6	1	5	10176.186	3	4	−0.002	10176.179	3	3	−0.006
6	2	5	10176.175	1	2	−0.002	10176.177		1	0.004
6	2	4	10216.619	1	3	0.001	10216.618		1	0.003
6	3	4	10216.306	1	2	−0.002	10216.303	4	3	−0.001
6	3	3	10248.568	4	5	0.007	10248.564	4	2	0.004
6	4	3	10244.860	2	3	0.011	10244.839	4	3	−0.009
6	4	2	10261.839	3	4	−0.001	10261.839	2	2	0.001
6	5	2	10276.440	6	3	0.005	10276.434	3	4	−0.001
6	5	1	10279.178	2	4	0.003	10279.176	4	2	0.003
6	6	1	10306.923	2	2	−0.001	10306.920	4	3	−0.001
6	6	0	10307.062	1	2	0.001	10307.061	2	2	0.001
7	0	7	10193.376	1	3	0.002	10193.375		1	0.005
7	1	7	10193.376	1	3	0.001	10193.375		1	0.005
7	1	6	10252.363	1	3	0.002	10252.369	2	3	0.002
7	2	6	10252.364	2	3	0.002	10252.363	1	2	−0.004
7	2	5	10301.528	2	3	−0.001	10301.509	2	5	0.003
7	3	5	10301.721	1	4	0.010	10301.710	4	2	0.001
7	3	4	10341.767	1	2	0.009	10341.759	4	3	0.005
7	4	4	10340.698	2	4	0.005	10340.697	4	2	0.006
7	4	3	10374.291	4	3	−0.010	10374.267	3	4	−0.012
7	5	3	10366.689	4	3	−0.004	10366.689	6	2	−0.004
7	5	2	10383.952	3	2	0.002	10383.949	1	3	0.000
7	6	2	10405.297	1	2	−0.002	10405.297	1	2	−0.002

Table 2 (*continued*)

J	K_a	K_c	$(40^-, 0)$				$(40^+, 0)$			
			E_{obs}	σ	N	Δ	E_{obs}	σ	N	Δ
7	6	1	10406.699	6	2	0.005	10406.689	2	2	−0.004
7	7	1	10440.808	1	2	−0.007				
7	7	0	10440.863	3	2	−0.005	10440.869		1	0.002
8	0	8	10269.405	2	3	0.004	10269.398		1	0.001
8	1	8	10269.406	2	3	0.004	10269.398		1	0.001
8	1	7	10337.441	2	3	−0.001	10337.437	1	2	−0.006
8	2	7	10337.438	4	4	0.000	10337.437	1	2	−0.002
8	2	6	10395.804	3	4	−0.003	10395.797	4	2	0.005
8	3	6	10395.800	5	4	−0.004	10395.807	4	4	0.012
8	3	5	10444.510	3	4	−0.006	10444.557*		1	0.031
8	4	5	10444.352	3	3	−0.003	10444.275	5	3	0.014
8	4	4	10484.196	3	4	0.009	10484.185	1	2	−0.008
8	5	4	10481.401	4	2	−0.005	10481.411	6	3	0.008
8	5	3	10518.161	4	3	0.003	10518.161	3	2	0.001
8	6	3	10504.935	4	2	−0.001	10504.942	3	2	0.009
8	6	2	10552.907	1	2	−0.008	10552.922	8	2	0.005
8	7	2	10524.368		1	−0.001	10524.377	4	4	0.001
8	7	1	10553.563	2	2	−0.002	10553.559	7	2	−0.003
8	8	1	10593.723	3	2	0.000	10593.726	3	3	0.002
8	8	0	10593.742	1	2	0.000				
9	0	9	10354.319	2	2	−0.001	10354.317		1	0.001
9	1	9	10354.319	2	2	−0.001	10354.317		1	0.001
9	1	8	10431.385	1	2	0.000	10431.379	5	2	−0.001
9	2	8	10431.384	1	2	−0.001	10431.379	5	2	−0.001
9	2	7	10498.701	2	2	0.000	10498.699	4	2	0.003
9	3	7	10498.704	5	4	0.004	10498.697	2	2	0.001
9	3	6	10556.321	1	2	0.004				
9	4	6	10556.274	2	3	0.003				
9	4	5	10604.288	3	3	−0.013	10604.266*	1	2	−0.031
9	5	5	10603.508*	4	4	−0.034				
9	5	4	10644.039	1	2	0.009	10644.042	2	3	0.013
9	6	4	10638.202	5	3	0.002				
9	6	3	10660.007	2	2	0.002	10659.988	1	3	−0.013
9	7	3	10719.415	1	2	0.002				
9	7	2	10719.157		1	0.010	10719.132	4	2	0.016
9	8	2	10683.701*	3	2	−0.023	10683.731		1	0.004
9	8	1	10680.155	3	2	0.002	10680.181*	2	3	0.028
9	9	1	10765.509	4	2	0.001				
9	9	0					10765.516		1	−0.005
10	0	10	10448.115		1	0.000	10448.103		1	−0.006
10	1	10	10448.115		1	0.000	10448.103		1	−0.006
10	1	9	10534.182	1	2	0.001	10534.173	6	2	−0.003
10	2	9	10534.182	1	2	0.000	10534.173	6	2	−0.003
10	2	8	10610.408	2	3	0.001	10610.403	2	2	0.001
10	3	8	10610.409	3	3	0.002	10610.403	2	2	0.000
10	3	7	10676.903	5	4	0.005	10676.897	2	3	0.009
10	4	7	10676.899		1	0.003	10676.898	2	2	0.011
10	4	6	10733.660	2	3	0.003	10733.662		1	0.008
10	5	6	10733.485	4	3	0.004				
10	5	5	10780.946	3	2	−0.009				
10	6	5	10778.919	5	2	−0.017	10778.918		1	−0.014
10	6	4	10821.025	4	2	−0.002				
10	7	4	10810.037	1	2	−0.017	10810.046	2	2	−0.007
10	7	3	10832.656	3	3	−0.013	10832.686	3	2	0.013
10	8	3	10904.297		1	−0.003	10904.292	3	2	−0.016
10	8	2	10904.172	1	2	−0.010				
10	9	2	10862.042		1	0.004	10862.044	3	2	0.002
10	9	1	10860.195	1	2	−0.004	10860.197		1	−0.005
10	10	1	10956.077		1	0.013				
10	10	0	10956.066		1	−0.001				
11	0	11	10550.773	3	2	0.003	10550.761		1	−0.004
11	1	11	10550.773	3	2	0.003	10550.761		1	−0.004

Table 2 (*continued*)

J	K_a	K_c	$(40^-, 0)$				$(40^+, 0)$			
			E_{obs}	σ	N	Δ	E_{obs}	σ	N	Δ
11	1	10	10645.813	2	2	0.002	10645.826		1	0.009
11	2	10	10645.813	2	2	0.002	10645.826		1	0.009
11	2	9	10730.920	1	2	0.006	10730.913	7	2	0.005
11	3	9	10730.920	1	2	0.007	10730.913	7	2	0.005
11	3	8	10806.226	2	2	0.001	10806.221	11	2	0.002
11	4	8	10806.232	2	4	0.006	10806.220	8	3	0.001
11	4	7					10871.779	5	3	0.017
11	5	7	10871.782	5	3	−0.015	10871.807	1	2	0.006
11	5	6	10927.648	1	2	0.008	10927.651*		1	0.019
11	6	6	10927.090	2	2	0.001				
11	6	5	10974.500*	3	2	0.024				
11	7	5	10969.906	4	2	0.003				
11	8	4	10998.440	6	2	0.003				
11	8	3	11023.145		1	0.001				
11	11	1	11165.486		1	0.000				
11	11	0	11165.481		1	−0.006				
12	0	12	10662.269		1	0.000	10662.252		1	−0.011
12	1	12	10662.269		1	0.000	10662.252		1	−0.011
12	1	11	10766.269		1	0.003	10766.266	1	2	−0.006
12	2	11	10766.269		1	0.003	10766.266	1	2	−0.006
12	2	10	10860.203	3	3	0.003	10860.197	6	2	0.003
12	3	10	10860.203	4	3	0.003	10860.197	6	2	0.003
12	3	9	10944.288	5	2	0.007	10944.284		1	0.010
12	4	9	10944.284	1	2	0.002	10944.283		1	0.010
12	4	8	11018.629	3	2	0.011	11018.629		1	0.011
12	5	8	11018.629		1	−0.001	11018.632		1	0.002
12	5	7	11083.106*		1	0.028				
12	6	7					11083.229		1	−0.017
12	8	4	11229.155	4	2	−0.007				
13	0	13	10782.595	2	2	0.002	10782.587		1	0.002
13	1	13	10782.595	2	2	0.002	10782.587		1	0.002
13	1	12	10895.527	1	2	−0.004	10895.521	3	2	−0.001
13	2	12	10895.527	1	2	−0.004	10895.521	3	2	−0.001
13	2	11	10998.257		1	0.001	10998.248		1	0.003
13	3	11	10998.257	1	2	0.001	10998.248		1	0.003
13	3	10	11091.062	1	2	0.001	11091.048	2	2	−0.001
13	4	10	11091.061	1	2	0.000	11091.048	2	2	−0.001
13	4	9					11174.131		1	−0.018
13	5	9	11174.131*		1	−0.018				
13	5	8					11247.607		1	−0.003
13	6	8	11247.607		1	0.003				
13	7	7	11311.458		1	0.006				
14	0	14	10911.723		1	0.002	10911.707		1	−0.004
14	1	14	10911.723		1	0.002	10911.707		1	−0.004
14	1	13	11033.569	7	2	−0.002	11033.555	3	2	−0.004
14	2	13	11033.569	7	2	−0.002	11033.555	3	2	−0.004
14	2	12	11145.044		1	0.002	11145.044		1	−0.014
14	3	12	11145.044		1	0.002	11145.044		1	−0.014
14	3	11	11246.528	7	2	−0.008				
14	4	11	11246.528	6	2	−0.008				
15	0	15	11049.636		1	0.006	11049.616		1	−0.001
15	1	15	11049.636		1	0.006	11049.616		1	−0.001
15	1	14	11180.371		1	0.002	11180.361		1	0.009
15	2	14	11180.366	5	2	−0.003	11180.361		1	0.009
15	2	13	11300.589		1	0.000				
15	3	13	11300.589		1	0.000				
16	0	16	11196.324*		1	0.030	11196.278		1	−0.002
16	1	16	11196.324*		1	0.030	11196.278		1	−0.002
16	1	15	11335.899		1	0.000	11335.873		1	−0.002
16	2	15	11335.899		1	0.000	11335.873		1	−0.002
17	0	17					11351.690		1	0.001

Table 2 (*continued*)

J	K_a	K_c	$(40^-, 0)$				$(40^+, 0)$			
			E_{obs}	σ	N	Δ	E_{obs}	σ	N	Δ
17	1	17					11351.690		1	0.001
18	0	18					11515.753		1	−0.009
18	1	18					11515.753		1	−0.009

Note. Asterisks denote the energy levels not included in the fit. σ denotes the experimental uncertainty of the level in 10^{-3} cm^{-1}. N is the number of observed transitions used to calculate the upper energy level. Δ is the difference between the experimental and calculated values of the energy in cm^{-1}.

Table 3
Rotational energy levels (cm^{-1}) of the $(30^-, 2)$, $(30^+, 2)$, $(20^-, 4)$, and $(11^+, 4)$ vibrational states of $H_2{}^{32}S$

J	K_a	K_c	$(30^-, 2)$				$(30^+, 2)$				$(20^-, 4)$			
			E_{obs}	σ	N	Δ	E_{obs}	σ	N	Δ	E_{obs}	σ	N	Δ
0	0	0	9806.667		1	0.006	9806.733		1	−0.004	9647.167		1	0.000
1	0	1	9820.091	6	2	0.002	9820.170*		1	0.022	9661.231	1	2	−0.001
1	1	1	9821.725		1	−0.001	9821.788	1	2	−0.003	9663.144		1	0.005
1	1	0	9826.305	5	2	0.003	9826.377	3	2	−0.003	9668.445	7	2	−0.003
2	0	2	9843.620	1	3	−0.003	9843.652	1	2	0.005	9685.478	4	2	0.007
2	1	2	9844.003	1	2	0.001	9844.027	2	3	−0.001	9685.746	5	3	−0.009
2	1	1	9857.712	4	3	−0.005	9857.775		1	0.000	9701.876	2	3	−0.004
2	2	1	9862.618	3	2	0.004	9862.683	1	2	−0.004	9707.542	3	3	0.004
2	2	0	9865.911	3	3	−0.001	9865.998		1	0.002	9711.353	1	2	−0.013
3	0	3	9875.631		1	0.002	9875.711		1	−0.010	9717.997	8	3	0.006
3	1	3	9875.620	1	3	−0.001	9875.709		1	−0.005	9718.013	5	2	−0.012
3	1	2	9901.112	1	2	−0.004	9901.148	2	3	0.006	9747.660	6	3	0.001
3	2	2	9902.863	1	4	−0.001	9902.887	3	2	−0.007	9749.772	5	3	0.006
3	2	1	9914.341	2	3	0.001	9914.401	3	3	0.003	9763.031		1	0.004
3	3	1	9924.051	1	2	0.006	9924.130	1	2	0.004	9774.186	1	3	−0.004
3	3	0	9926.041	1	3	0.007	9926.123	1	2	0.000	9776.498	1	2	−0.003
4	0	4	9916.301	1	4	−0.003	9916.375		1	−0.001	9759.061	6	3	0.001
4	1	4	9916.298	1	3	−0.001	9916.374		1	0.003	9759.058		1	−0.005
4	1	3	9953.156	2	4	−0.002	9953.557		1	0.007	9801.918	2	3	0.005
4	2	3	9953.148	3	2	0.001	9953.537	3	3	−0.003	9802.102	2	3	0.006
4	2	2	9976.809	4	3	0.000	9976.845	2	2	0.009	9829.370	2	2	−0.002
4	3	2	9981.477	1	3	0.001	9981.503	2	3	−0.007	9834.864	4	3	−0.005
4	3	1	9990.254	3	5	0.001	9990.319	3	2	0.006	9844.992	1	2	0.010
4	4	1	10006.065	2	2	0.002	10006.147	7	2	−0.005	9863.071		1	0.005
4	4	0	10007.095	5	2	0.005	10007.185		1	0.000	9864.270	4	3	0.003
5	0	5	9965.780	2	3	−0.007	9965.854		1	−0.004	9808.824	4	2	0.008
5	1	5	9965.782	2	3	−0.004	9965.854		1	−0.003	9808.817	3	2	0.003
5	1	4	10013.453	3	3	0.004	10013.552	2	2	0.000	9864.182	6	2	−0.010
5	2	4	10013.431	2	4	0.008	10013.535	1	2	0.009	9864.205	4	3	0.002
5	2	3	10050.533	6	3	0.001	10050.555	5	4	0.007	9905.505	17	2	0.000
5	3	3	10049.108	4	4	0.010	10049.104	5	3	−0.001	9907.246	1	3	−0.002
5	3	2	10070.627	5	4	−0.001	10070.660	2	3	0.003	9930.482	1	2	−0.008
5	4	2	10079.937	4	4	0.001	10079.967		1	0.006	9941.365		1	0.003
5	4	1	10085.925	1	2	−0.001	10085.987		1	0.004	9948.243		1	0.000
5	5	1	10108.644	5	2	−0.001	10108.745		1	0.003	9974.044	2	2	0.004
5	5	0	10109.123	4	2	−0.009	10109.224	3	4	−0.005	9974.600		1	−0.005
6	0	6	10024.085	5	3	−0.001	10024.162		1	0.008	9867.271		1	0.002
6	1	6	10024.082	5	3	−0.003	10024.162		1	0.008	9867.272		1	0.003
6	1	5	10082.364	4	4	−0.001	10082.442	1	2	−0.007	9934.997	3	3	−0.006
6	2	5	10082.356	7	3	−0.001	10082.441	1	3	−0.001	9935.000		1	0.001
6	2	4	10129.538	2	4	−0.003	10129.576	4	2	−0.003	9989.325	2	3	−0.013
6	3	4	10129.208	1	2	−0.001	10129.248	4	3	−0.001	9989.403	1	2	0.020
6	3	3	10166.634	4	3	−0.003	10166.606	2	3	−0.005	10028.073	3	2	−0.005
6	4	3	10162.832	3	2	−0.002	10162.835	5	3	0.000				
6	4	2	10182.841	5	3	0.003	10182.874		1	0.001	10051.274	1	2	−0.004
6	5	2	10198.212		1	0.007	10198.320	4	2	0.001	10069.239		1	−0.003
6	5	1	10201.691	1	2	−0.006	10201.956	6	2	−0.001	10073.394	10	4	0.012
6	6	1	10231.668	1	2	−0.008	10231.791	1	2	−0.003				
6	6	0	10231.879	6	3	−0.004	10232.005		1	0.002	10107.105	3	2	−0.010

Table 3 (*continued*)

J	K_a	K_c	$(30^-, 2)$				$(30^+, 2)$				$(20^-, 4)$			
			E_{obs}	σ	N	Δ	E_{obs}	σ	N	Δ	E_{obs}	σ	N	Δ
7	0	7	10091.194	3	2	−0.005	10091.260		1	−0.002	9934.411	6	2	−0.007
7	1	7	10091.193	3	2	−0.005	10091.260		1	−0.002	9934.411	6	2	−0.007
7	1	6	10160.061	5	3	−0.005	10160.156	4	3	0.004	10014.489	5	3	−0.002
7	2	6	10160.064	2	3	−0.001	10160.153	5	3	0.003	10014.489	8	4	0.000
7	2	5	10217.597	7	2	0.008	10217.705	3	2	−0.001	10081.056	1	2	−0.002
7	3	5	10217.540	4	3	−0.014	10217.643*		1	−0.026	10081.052	2	3	0.013
7	3	4	10264.198		1	−0.005	10264.239	4	3	−0.003				
7	4	4	10263.128	4	4	0.006	10263.166	3	4	0.008	10133.847	4	2	−0.007
7	4	3	10302.100	4	4	−0.014	10293.921	2	2	−0.003	10169.006	3	2	0.000
7	5	3	10302.089	5	2	−0.009	10293.932	6	3	0.009	10178.169	8	2	0.004
7	5	2	10313.629	1	4	−0.012	10313.917	3	2	−0.011				
7	6	2	10336.485	2	4	0.001	10336.605	3	2	0.004	10218.430	2	2	0.003
7	6	1					10338.579		1	0.003	10220.700		1	0.004
7	7	1	10375.035	8	3	0.005	10375.207	4	3	0.005	10261.103	3	2	−0.001
7	7	0	10375.039	6	3	−0.002	10375.230	4	2	−0.005	10261.218*		1	−0.035
8	0	8	10167.082	4	3	0.006	10167.152		1	0.006	10010.267	6	2	0.011
8	1	8	10167.082	4	3	0.006	10167.152		1	0.006	10010.267	6	2	0.011
8	1	7	10246.316	5	4	−0.001	10247.070*	3	2	0.027	10102.660		1	−0.019
8	2	7	10246.315	4	3	−0.008	10247.070	3	2	0.001	10102.662		1	−0.017
8	2	6	10314.548	4	3	−0.005	10314.647	9	2	−0.011	10181.325	4	3	−0.002
8	3	6	10314.540	6	3	0.001	10314.647	10	2	−0.001	10181.322		1	0.005
8	3	5	10371.262		1	−0.005	10371.335		1	−0.010	10246.073	5	2	0.001
8	4	5	10370.968	2	2	−0.008	10371.059	3	3	0.002				
8	4	4	10417.375	5	3	0.007	10417.413		1	−0.004	10296.605		1	0.006
8	5	4	10414.430	1	2	−0.001	10414.506	3	2	0.000				
8	5	3	10441.828	6	4	0.007	10456.279		1	0.010	10328.284		1	0.008
8	6	3	10442.327*		1	−0.041	10456.353	6	2	0.003				
8	6	2	10464.224	2	3	0.009	10464.441		1	−0.011	10353.912	3	2	−0.017
8	7	2	10494.648	3	2	0.019	10494.917		1	0.005				
8	7	1	10495.554	3	2	0.002	10495.880		1	−0.002				
8	8	1	10538.246		1	0.007	10538.718		1	−0.002	10436.449*		1	−0.017
8	8	0	10538.275	4	2	0.001	10538.758		1	0.001	10436.452		1	0.003
9	0	9	10251.765	6	3	−0.002	10251.833		1	−0.003	10094.725		1	0.000
9	1	9	10251.765	6	3	−0.002	10251.833		1	−0.003	10094.725		1	0.000
9	1	8	10341.786	6	3	0.009	10341.876	7	2	−0.001	10199.581		1	0.005
9	2	8	10341.785	5	3	0.009	10341.876	7	2	−0.001	10199.581		1	0.005
9	2	7	10420.119	3	2	0.000	10420.252		1	−0.008	10290.222	5	3	0.002
9	3	7	10420.117	1	2	0.008	10420.252		1	−0.001	10290.225	6	3	0.008
9	3	6					10487.574	5	2	0.002				
9	4	6	10487.204	2	3	−0.009					10367.257		1	−0.004
9	4	5	10543.013	4	2	0.006	10543.164*		1	−0.042				
9	5	5	10542.106	2	2	−0.001								
	5	4					10589.106		1	0.009				
9														
9	6	4	10582.619	5	3	0.006								
9	7	2	10634.719		1	−0.011	10633.933		1	0.009				
9	8	2	10672.409	1	2	−0.014								
9	8	1					10629.653	2	2	−0.005				
9	9	1	10721.339	2	2	−0.003								
10	0	10	10345.225	4	3	−0.003	10345.294		1	−0.004	10187.960		1	−0.005
10	1	10	10345.225	4	3	−0.003	10345.294		1	−0.004	10187.960		1	−0.005
10	1	9	10445.812	3	3	0.004	10445.915	6	2	0.004				
10	2	9	10445.812	3	3	0.004	10445.915	6	2	0.004				
10	2	8	10534.532	4	2	−0.008	10534.802*	5	2	0.100				
10	3	8	10534.532	5	2	−0.006	10534.802*	5	2	0.101				
10	3	7	10611.683	4	2	−0.011					10496.560		1	0.005
10	4	7	10611.676	5	2	0.005					10496.547		1	0.006
10	4	6	10677.355*	2	2	−0.083								
10	6	5					10729.369	3	2	−0.007				
10	6	4	10778.665	5	2	−0.002								
10	7	3	10793.028	1	2	0.002								
10	8	3					10870.058	7	2	0.005				

Table 3 (*continued*)

J	K_a	K_c	$(30^-,2)$				$(30^+,2)$				$(20^-,4)$			
			E_{obs}	σ	N	Δ	E_{obs}	σ	N	Δ	E_{obs}	σ	N	Δ
10	10	1	10923.682		1	0.008								
10	10	0	10923.669	1	2	−0.009								
11	0	11	10447.448	5	2	−0.002	10447.516		1	−0.004	10289.814		1	0.001
11	1	11	10447.448	5	2	−0.002	10447.516		1	−0.004	10289.814		1	0.001
11	1	10	10558.602	4	3	0.005	10558.707	6	2	0.006	10419.529		1	0.006
11	2	10	10558.602	4	3	0.005	10558.707	6	2	0.006	10419.529		1	0.006
11	2	9	10657.725*	5	2	0.068	10657.857	7	2	0.005	10534.032		1	−0.009
11	3	9	10657.724*	4	2	0.067	10657.857	8	2	0.005	10534.032		1	−0.009
11	3	8	10744.948*		1	−0.045								
11	4	8	10744.950*	1	2	−0.039								
11	5	7	10820.744	6	2	0.002								
12	0	12	10558.423	4	2	0.005	10558.496	6	2	0.005				
12	1	12	10558.423	4	2	0.005	10558.496	6	2	0.005				
12	1	11	10680.136	4	3	0.002	10680.241		1	0.000				
12	2	11	10680.136	4	3	0.002	10680.241		1	0.000				
12	2	10	10789.516*	4	2	0.027	10789.704*		1	−0.033	10669.008		1	0.001
12	3	10	10789.516*	4	2	0.027	10789.704*		1	−0.033	10669.008		1	0.001
13	0	13	10678.123	1	2	0.004	10678.192		1	0.000				
13	1	13	10678.123	1	2	0.004	10678.192		1	0.000				
13	1	12	10810.402	2	2	−0.006	10810.520		1	−0.001				
13	2	12	10810.402	2	2	−0.006	10810.520		1	−0.001				
13	2	11	10930.035	6	2	0.001								
13	3	11	10930.035	5	3	0.000								
14	0	14	10806.530		1	−0.005	10806.604		1	−0.004				
14	1	14	10806.530		1	−0.005	10806.604		1	−0.004				
14	1	13	10949.407		1	0.002								
14	2	13	10949.407		1	0.002								
14	2	12					11079.799		1	−0.001				
14	3	12					11079.799		1	−0.001				
15	0	15	10943.648		1	−0.001	10943.727		1	0.003				
15	1	15	10943.648		1	−0.001	10943.727		1	0.003				
			$(11^+,4)$											
8	6	3	10444.693	5	2	−0.004								
9	7	2	10637.662	1	2	−0.004								

Note. Asterisks denote the energy levels not included in the fit. σ denotes the experimental uncertainty of the level in $10^{-3}\,cm^{-1}$. N is the number of observed transitions used to calculate the upper energy level. Δ is the difference between the experimental and calculated values of the energy in cm^{-1}.

$$H^C = C_{xz}\{J_x,J_z\} + C_{xzj}\{J_x,J_z\}J^2 + C_{xzjj}\{J_x,J_z\}J^4 + C_{xzkj}\{J_x,J_z^3\}J^2 + C_{yk}\{iJ_y,J_z^2\} + \cdots \quad (2)$$

with $\{A,B\} = AB + BA$ and $J_{xy}^2 = J_x^2 - J_y^2$.

The considered vibrational states belong to the first pentadecade of interacting states, if we follow the conventional polyad structure for water-like molecules. Among the fifteen vibrational states included in this pentadecade, nine are located in the analyzed spectral region and could contribute to the observed spectrum. They are the $(20^-,4)$, $(20^+,4)$, $(11^+,4)$, $(30^-,2)$, $(30^+,2)$, $(40^-,0)$, $(40^+,0)$, $(21^+,2)$, and $(21^-,2)$ states with vibrational energies predicted [10] at 9646.814, 9647.248, 9745.777, 9806.461, 9806.574, 9911.043, 9911.059, 9993.438, and 10 004.541 cm^{-1}, respectively. Preliminary calculations performed with rotational parameters estimated from lower vibrational states [10] have shown that the $(11^+,4)$ and $(20^+,4)$ dark states should be included into consideration since they perturb significantly some of the experimentally observed states (see below). On the other hand, the $(21^+,2)$ and $(21^-,2)$ states, though being only 82 and 93 cm^{-1} higher in energy than the $(40^\pm,0)$ bright states, have higher bending excitation leading to a rapid detuning of the rotational levels compared to those of the $(40^\pm,0)$ LM pair. In consequence, these two states were not included in the effective Hamiltonian model and only the subset of seven states listed in Table 1 was considered. They consist in three nearly local mode pairs—$(20^\pm,4)$, $(30^\pm,2)$, $(40^\pm,0)$—and the $(11^+,4)$ separate state.

As previously studied experimentally and theoretically (see [9] and references quoted therein), at the local mode limit, the rotational structure is predicted to be identical for the two components of a LM pair, the Coriolis resonance parameter C_y between the two components vanishes and, in case of interaction between two LM pairs, similar resonance parameters should be identical. In the present case, no one of the studied LM pairs could be considered as a strict LM pair: the

Table 4
Vibrational energies and rotational and coupling constants for the $(40^{\pm}, 0)$, $(30^{\pm}, 2)$, $(20^{\pm}, 4)$, and $(11^{+}, 4)$ vibrational states of $H_2{}^{32}S$, $H_2{}^{33}S$, and $H_2{}^{34}S$.
$H_2{}^{32}S$: 683 energy levels (654 included in the fit), 84 adjusted parameters (30 resonance and 54 diagonal), rms: $0.0061\,cm^{-1}$

$H_2{}^{32}S$	$(40^-, 0)$	$(40^+, 0)$	$(30^-, 2)$	$(30^+, 2)$	$(20^-, 4)$	$(20^+, 4)$	$(11^+, 4)$
E_v	9911.023710(2100)	9911.0194490(9200)	9806.660901(2400)	9806.737202(2500)	9647.167216(3000)	9647.77480(2500)	9744.88812(2900)
A	9.6673256(3100)		10.4778561(5700)	10. 4819222(5500)	11.5291843(9400)	11.622228(2200)	11.565604(2600)
B	8.5635393(1100)		9.1670864(3900)	9.1654446(4400)	9. 7602913(9400)	9.737	9.769
C	4.47603022(4200)		4.41872748(7500)	4. 418111085(8000)	4.3549973(2200)	4.3447418(2600)	4.395
Δ_k	$3.38237(1100) \times 10^{-3}$		$5.49316(1300) \times 10^{-3}$	$5.684617(1500) \times 10^{-3}$	$6.6638(1400) \times 10^{-3}$	9.40×10^{-3}	$7.7093(1000) \times 10^{-3}$
Δ_{jk}	$-1.220395(3800) \times 10^{-3}$		$-3.47217(1000) \times 10^{-3}$	$-3.47785(1100) \times 10^{-3}$	$-3.66514(7700) \times 10^{-3}$	-4.84×10^{-3}	$-3.90911(5700) \times 10^{-3}$
Δ_j	$3.392678(1900) \times 10^{-4}$		$8.849960(5900) \times 10^{-4}$	$8.698304(6700) \times 10^{-4}$	$1.24315(1000) \times 10^{-3}$	1.22×10^{-3}	1.22×10^{-3}
δ_k	$-1.14213(1900) \times 10^{-4}$				$1.24679(3200) \times 10^{-3}$	5.53×10^{-4}	5.53×10^{-4}
δ_j	$1.341842(1300) \times 10^{-4}$		$4.127841(3400) \times 10^{-4}$	$4.052017(3500) \times 10^{-4}$	$5.84446(2900) \times 10^{-4}$	5.80×10^{-4}	5.80×10^{-4}
H_k	$1.12309(7500) \times 10^{-6}$		$2.2604(1100) \times 10^{-6}$	$5.6113(1100) \times 10^{-6}$	$2.01611(3500) \times 10^{-5}$	1.70×10^{-5}	1.70×10^{-5}
H_{kj}	1.18×10^{-6}		-2.84×10^{-8}	-2.84×10^{-8}	-2.13×10^{-6}	-2.13×10^{-6}	-2.13×10^{-6}
H_{jk}	-1.45×10^{-6}		$-1.78082(6200) \times 10^{-6}$	$-2.61153(5600) \times 10^{-6}$	-3.22×10^{-6}	-3.22×10^{-6}	-3.22×10^{-6}
H_j	2.68×10^{-7}		5.29×10^{-7}	5.29×10^{-7}	$8.1019(2500) \times 10^{-7}$	8.86×10^{-7}	8.86×10^{-7}
h_k	$1.92339(2500) \times 10^{-6}$		$3.3728(1000) \times 10^{-6}$	$3.27(1000) \times 10^{-6}$	$1.47572(2500) \times 10^{-5}$	7.78×10^{-6}	7.78×10^{-6}
h_{kj}	-4.60×10^{-7}		$-7.3702(3200) \times 10^{-7}$	$-7.22(3200) \times 10^{-7}$	$-3.1664(1100) \times 10^{-6}$	-1.30×10^{-6}	-1.30×10^{-6}
h_j	1.34×10^{-7}		2.65×10^{-7}	2.65×10^{-7}	4.41×10^{-7}	4.41×10^{-7}	4.41×10^{-7}
L_k	-3.56×10^{-9}		-1.70×10^{-8}	-1.70×10^{-8}	-1.60×10^{-7}	-1.60×10^{-7}	-1.60×10^{-7}
L_{kj}	4.44×10^{-9}		2.12×10^{-8}	2.12×10^{-8}	7.05×10^{-8}	7.05×10^{-8}	7.05×10^{-8}

Coupling constants for $H_2{}^{32}S$

	$F_k \times 10^2$	$F_j \times 10^2$
$(30^-, 2)$–$(40^-, 0)$	1.45465(3700)	2.82026(3200)
$(40^+, 0)$–$(30^+, 2)$	1.53515(2600)	2.79966(1100)
$(11^+, 4)$–$(30^+, 2)$	−1.37138(5500)	−1.64260(1800)

	$C_{xzk} \times 10^4$	$C_{yk} \times 10^5$	$C_{xz} \times 10^2$	$C_{xzj} \times 10^4$	$C_{xzkj} \times 10^6$	$C_{xzjj} \times 10^6$
$(30^+, 2) - (20^-, 4)$	−8.6800(1400)		1.6328(1400)	3.0980(2100)		
$(30^+, 2) - (40^-, 0)$			−2.57804(7500)	1.72811(9900)		
$(30^+, 2) - (30^-, 2)$		8.6424(7600)	−48.83210(4600)			
$(40^+, 0) - (40^-, 0)$	−3.80850(4500)		−51.77609(1900)	−4.51853(3700)	4.45897(3900)	−1.06601(2200)
$(40^+, 0) - (30^-, 2)$			−2.84623(7300)	2.1094(1000)		
$(20^+, 4) - (20^-, 4)$	17.208(1600)		−33.6733(2000)			4.1356(5100)
$(20^+, 4) - (30^-, 2)$	−7.8479(4800)		2.3682(2600)	2.9640(3600)		
$(11^+, 4) - (20^-, 4)$			−6.88843(6200)			
$(11^+, 4) - (40^-, 0)$	1.99020(6000)					
$(11^+, 4) - (30^-, 2)$	−5.2058(2000)			1.2148(1100)		

Minor isotopomers[a]
$H_2{}^{33}S$: 28 energy levels (27 included in the fit), 3 adjusted parameters, standard deviation: $0.010\,cm^{-1}$

$H_2{}^{33}S$	$(40^{\pm}, 0)$	$(30^-, 2)$	$(30^+, 2)$	$(20^-, 4)$	$(20^+, 4)$	$(11^+, 4)$
E_v	9907.050108(7700)	9802.7012	9802.7668	9643.0336	9643.8174	9740.8740
A	9.6170666(7400)	10.45901	10.46307	11.50845	11.60132	11.54480
B	8.591797(2100)	9.167061	9.165419	9.760263	9.736973	9.768972
C	4.47229100	4.415036	4.414420	4.351358	4.341112	4.391328
Δ_k	3.3752×10^{-3}	5.4816×10^{-3}	5.6726×10^{-3}	6.6497×10^{-3}	9.3802×10^{-3}	7.6930×10^{-3}

Table 4 (*continued*)

$H_2{}^{34}S$: 181 energy levels (175 included in the fit), 11 adjusted parameters, standard deviation: $0.0068\,cm^{-1}$

$H_2{}^{34}S$	$(40^-,0)$	$(40^+,0)$	$(30^-,2)$	$(30^+,2)$	$(20^-,4)$	$(20^+,4)$	$(11^+,4)$
E_v	9903.320290(1800)	9903.313489(1100)	9798.741532(2300)	9798.796482(4500)	9638.90	9639.86	9736.86
A	9.6326142(1200)		10.4398208(2200)	10.445430	11.48904	11.58176	11.52533
B	8.56563808(6200)		9.167038	9.1665765(6300)	9.760240	9.736949	9.768949
C	4.46903478(1800)		4.41176398(4600)	4.41112214(8200)	4.347974	4.337735	4.387912
Δ_k	3.3676×10^{-3}		5.4692×10^{-3}	5.6598×10^{-3}	6.6347×10^{-3}	9.3590×10^{-3}	7.6756×10^{-3}

Note. All the results are in cm^{-1} and quoted errors are one standard deviation. Parameters presented without quoted errors were constrained to the given value (see text).

[a] All the other diagonal and resonance vibrational parameters were fixed to the $H_2{}^{32}S$ values.

$(40^{\pm},0)$ states have very close but not absolutely coinciding rotational structure, the rotational levels of the $(30^{\pm},2)$ pair differ by about $0.077\,cm^{-1}$ while the separation between the components of the $(20^{\pm},4)$ pair is even larger and reaches a value of $0.607\,cm^{-1}$. Consequently, in the process of refinement of the Hamiltonian parameters, we could not keep identical the rotational and centrifugal distortion parameters of the components of the LM pairs without a noticeable loss in the quality of the energy levels reproduction. Thus, we varied independently the vibrational energies E_v of the $(40^{\pm},0)$ states as well as all rotational and centrifugal distortion parameters for the other LM pairs. As a consequence, of the strong resonance coupling with the bright states three and four parameters were varied for the $(20^+,4)$ and $(11^+,4)$ dark states, respectively, leading to values which might be considered as effective as, in fact, only two energy levels of the $(11^+,4)$ dark state are experimentally determined (see below). We intend to adopt a resonance scheme which describes in a similar way and amplitude the resonance interaction between the LM pairs. Indeed, Table 4 shows that the resonance parameters between LM pairs, have close, though not coinciding values. For instance, the same coupling parameters with close values account for the interaction between the $(20^+,4)$ and $(30^-,2)$ states on one hand, and between the $(20^-,4)$ and $(30^+,2)$ states on the other hand.

An rms deviation of $0.0061\,cm^{-1}$ was achieved by varying 54 diagonal and 30 resonance parameters listed in Table 4 with 68% confidence intervals. Parameters without confidence interval were fixed to the corresponding values of the $(20^-,0)$ state for the $(40^{\pm},0)$ pair, of the $(10^-,2)$ state for the $(30^{\pm},2)$ pair, and of the $(00^+,4)$ state for the $(20^{\pm},4)$ pair and the $(11^+,4)$ state [14]. The necessity to account for strong interaction with two highly excited bending dark states—$(20^+,4)$ and $(11^+,4)$—led to a relative large number of varied resonance parameters: 10 of them concern indeed this interaction.

A remarkable example of strong resonance coupling is the interaction between the $(40^{\pm},0)$ [7 2 5] levels at 10 301.528 and 10 301.509 cm^{-1}, respectively, and the $(30^{\pm},2)$ [7 4 3] levels at 10 302.100 and 10 302.089 cm^{-1}, respectively. The resulting wavefunctions of these levels correspond to a nearly equal mixing of the four resonating states. A second example is the strong interaction between the $(11^+,4)$ dark state and the $(40^{\pm},0)$ and $(30^{\pm},2)$ pairs which induces an important intensity borrowing leading to the observation of extra lines reaching the $(11^+,4)$ [8 6 3] and $(11^+,4)$ [9 7 2] levels observed at 10 444.693 and 10 637.662 cm^{-1}, respectively (see Fig. 3). As mentioned above, this kind of "non-symmetric" interactions with, for instance, the single $(11^+,4)$ state, induces sometimes an increase of the energy separation between specific rotational levels of

Table 5
Rotational energy levels (cm^{-1}) of the $(40^-, 0)$ and $(40^+, 0)$ vibrational states of $H_2{}^{33}S$

J	K_a	K_c	$(40^-, 0)$				$(40^+, 0)$			
			E_{obs}	σ	N	Δ	E_{obs}	σ	N	Δ
2	0	2	9942.787		1	−0.014				
2	1	2					9943.143		1	0.005
2	2	0	9961.973	3	2	−0.009				
3	2	2	9997.721*		1	0.022				
4	0	4	10014.693		1	−0.007	10014.693		1	−0.006
4	1	4	10014.693		1	0.000	10014.693		1	−0.001
4	1	3	10046.542		1	−0.015				
5	0	5	10063.940	1	2	−0.006	10063.942	3	2	−0.003
5	1	5	10063.942	3	2	−0.002				
5	5	1	10187.369		1	0.001				
6	0	6	10122.109	4	2	0.009	10122.113		1	0.015
6	1	6	10122.105		1	0.005	10122.109	4	2	0.010
7	0	7	10189.176		1	0.001	10189.162		1	−0.012
7	1	7	10189.176		1	0.001	10189.162		1	−0.012
8	0	8	10265.155		1	0.014				
8	1	8	10265.155		1	0.014				
9	0	9					10349.998		1	0.009
9	1	9					10349.998		1	0.010
11	0	11	10546.270		1	−0.008	10546.261		1	−0.016
11	1	11	10546.270		1	−0.008				

Note. σ denotes the experimental uncertainty of the level in $10^{-3}\,cm^{-1}$. N is the number of observed transitions used to calculate the upper energy level. Δ is the difference between the experimental and calculated values of the energy in cm^{-1}.

Table 6
Rotational energy levels (cm^{-1}) of the $(40^-, 0)$ and $(40^+, 0)$ vibrational states of $H_2{}^{34}S$

J	K_a	K_c	$(40^-, 0)$				$(40^+, 0)$			
			E_{obs}	σ	N	Δ	E_{obs}	σ	N	Δ
0	0	0	9903.323		1	0.003				
1	0	1					9916.140		1	0.003
1	1	1	9917.637	2	2	0.007				
1	1	0	9921.512		1	−0.004				
2	0	2	9939.039		1	0.008				
2	1	2	9939.394		1	0.013	9939.386	3	2	0.005
2	1	1	9951.029	2	2	−0.001				
2	2	1					9955.494		1	0.009
2	2	0	9958.242	2	2	0.008				
3	0	3	9970.612		1	0.000	9970.604		1	−0.003
3	1	3	9970.558	1	2	0.000	9970.554		1	0.000
3	1	2	9992.270		1	−0.003	9992.275	9	3	0.003
3	2	2	9993.914	3	2	0.002	9993.911	1	2	−0.001
3	2	1	10003.546	2	2	−0.012	10003.547		1	−0.007
3	3	1	10012.415	1	2	0.005				
3	3	0					10014.010		1	0.002
4	0	4	10010.892		1	0.006				
4	1	3	10042.713	2	2	0.001				
4	2	3					10042.336	2	2	−0.010
4	2	2	10062.428		1	0.001	10062.419		1	−0.006
4	3	2	10066.772		1	−0.006	10066.781	5	2	0.003
4	3	1	10074.039	9	2	0.006	10074.031		1	0.002
4	4	1					10088.505*		1	0.026
4	4	0	10089.276	3	2	−0.004				
5	0	5	10060.087	3	2	−0.007	10060.089	5	2	0.002
5	1	5	10060.089	4	3	−0.004	10060.087	3	2	0.001
5	2	4	10100.837		1	−0.006				
5	2	3	10132.613		1	0.002	10132.598	5	2	−0.009
5	3	3	10131.267		1	0.001				
5	3	2					10149.477	2	2	−0.008
5	4	2	10158.095	1	2	−0.005	10158.124*		1	0.024
5	4	1	10162.919		1	−0.017	10162.936		1	0.004

Table 6 (*continued*)

J	K_a	K_c	(40⁻, 0)				(40⁺, 0)			
			E_{obs}	σ	N	Δ	E_{obs}	σ	N	Δ
5	5	1	10183.765	5	2	0.010				
5	5	0					10184.118		1	0.015
6	0	6	10118.206	3	3	0.002	10118.202		1	0.005
6	1	6	10118.205	4	2	0.001	10118.205	4	2	0.009
6	1	5	10168.074	3	3	−0.001				
6	2	5	10168.079		1	0.014	10168.070		1	0.012
6	2	4	10208.442		1	−0.006				
6	3	4	10208.153		1	−0.006				
6	4	3					10236.742		1	−0.010
6	4	2	10253.748	8	2	0.007				
6	5	2					10267.984	4	2	−0.014
6	6	0	10298.354		1	0.005				
7	0	7	10185.226	1	2	−0.004	10185.227		1	0.004
7	1	7	10185.226	1	2	−0.004	10185.227		1	0.004
7	1	6	10244.133		1	−0.002	10244.127	4	2	−0.001
7	2	6	10244.129	5	3	−0.006	10244.122		1	−0.005
7	2	5	10293.615		1	0.001	10293.590*		1	−0.020
7	3	5	10293.418	2	2	0.002				
7	4	4	10332.413	7	3	0.011				
7	5	3	10358.468*		1	−0.031				
7	5	2					10375.663		1	0.013
7	6	2	10396.553		1	−0.008				
7	7	1	10431.745		1	−0.008				
8	0	8	10261.138	2	3	−0.001	10261.135		1	0.003
8	1	8	10261.139		1	0.000	10261.135		1	0.003
8	1	7	10329.076	12	2	−0.001	10329.064		1	−0.006
8	2	7					10329.065	1	2	−0.006
8	2	6	10387.361	8	3	0.001				
8	3	6	10387.350	4	2	−0.005	10387.359		1	−0.001
8	3	5	10436.023		1	−0.008				
8	4	4	10475.610		1	0.012				
8	5	3	10509.391		1	0.003				
8	7	2					10515.793		1	0.004
9	0	9	10345.922		1	−0.003	10345.908		1	−0.008
9	1	9	10345.921		1	−0.003	10345.908		1	−0.008
9	1	8	10422.863	2	2	−0.009	10422.860	1	2	−0.005
9	2	8	10422.863	2	2	−0.009	10422.860	1	2	−0.005
9	2	7	10490.098		1	0.005	10490.092	1	3	0.006
9	3	7	10490.096	6	3	0.004	10490.092	1	2	0.006
9	3	6	10547.629		1	−0.007				
9	4	6	10547.597	1	2	0.003				
10	0	10	10439.586		1	0.014				
10	1	10	10439.586		1	0.014				
10	1	9	10525.507	7	2	−0.001	10525.500		1	−0.001
10	2	9	10525.513		1	0.005	10525.500		1	−0.001
10	2	8	10601.622	8	2	−0.001	10601.616		1	0.000
10	3	8	10601.623	7	2	0.000	10601.615		1	−0.002
11	0	11	10542.074		1	0.007	10542.052		1	−0.006
11	1	11	10542.074		1	0.007	10542.052		1	−0.006
11	1	10	10636.957		1	−0.012				
11	2	10	10636.957		1	−0.012				
12	0	12	10653.379		1	−0.012	10653.388		1	0.006
12	1	12	10653.379		1	−0.012	10653.388		1	0.006
12	2	10	10850.996*		1	−0.019				
12	3	10	10850.996*		1	−0.019				
13	0	13	10773.517		1	−0.010				
13	1	13	10773.517		1	−0.010				
13	2	11	10988.850		1	0.001				
13	3	11	10988.850		1	0.001				
14	0	14	10902.462		1	0.011				
14	1	14	10902.462		1	0.011				

Note. Asterisks denote the energy levels not included in the fit. σ denotes the experimental uncertainty of the level in 10^{-3} cm^{-1}. N is the number of observed transitions used to calculate the upper energy level. Δ is the difference between the experimental and calculated values of the energy in cm^{-1}.

Table 7
Rotational energy levels (cm^{-1}) of the $(30^-, 2)$ and $(30^+, 2)$ vibrational states of $H_2{}^{34}S$

J	K_a	K_c	$(30^-, 2)$				$(30^+, 2)$			
			E_{obs}	σ	N	Δ	E_{obs}	σ	N	Δ
1	0	1	9812.158		1	0.001				
2	0	2	9835.648		1	0.002				
2	1	1	9849.731		1	−0.009				
2	2	1	9854.558		1	0.011				
2	2	0	9857.861		1	−0.006				
3	0	3	9867.586		1	−0.011	9867.688		1	0.013
3	1	3	9867.588	3	2	−0.002				
3	2	2	9894.766		1	0.005				
3	2	1	9906.286	3	3	0.000				
3	3	1	9915.829	1	2	0.016				
4	0	4	9908.206		1	−0.002	9908.268		1	0.005
4	1	4	9908.206		1	0.003	9908.268		1	0.009
4	1	3					9945.381		1	0.000
4	2	3					9945.015		1	0.006
4	2	2	9968.690	8	2	0.001				
4	3	1	9982.065		1	−0.008				
4	4	1	9997.594		1	−0.011	9997.690		1	−0.009
4	4	0	9998.657		1	−0.001				
5	0	5	9957.614		1	0.002				
5	1	5	9957.614		1	0.003				
5	4	2	10071.471		1	0.012				
5	5	1	10099.905		1	0.005				
5	5	0	10100.374		1	−0.010				
6	0	6	10015.819	2	2	0.002	10015.862		1	−0.009
6	1	6	10015.817		1	0.000	10015.862		1	−0.009
6	1	5	10073.998		1	0.001	10074.079		1	−0.003
6	2	5	10073.999		1	0.010	10074.078		1	0.003
6	3	4					10120.834		1	−0.001
6	4	2	10174.475		1	−0.006				
7	0	7	10082.818	3	2	−0.005	10082.867		1	−0.007
7	1	7	10082.818	3	2	−0.005	10082.867		1	−0.007
8	2	6	10305.814	1	2	0.002				
9	1	9	10243.141		1	0.003				
9	2	8	10332.986		1	−0.008				
9	3	7	10411.204		1	0.004				
10	0	10	10336.448	8	2	−0.004				
10	1	10	10336.456		1	0.005	10336.522		1	0.011

Note. σ denotes the experimental uncertainty of the level in $10^{-3}\,cm^{-1}$. N is the number of observed transitions used to calculate the upper energy level. Δ is the difference between the experimental and calculated values of the energy in cm^{-1}.

the $(40^{\pm}, 0)$ LM states. For instance, the [8 4 5] energy levels are separated by $0.076\,cm^{-1}$. A similar situation was encountered and analyzed in our recent study of the $(40^{\pm}, 1)$—(0 0 0) overtone transition near $11\,000\,cm^{-1}$ [9].

As soon as the transitions of the main isotope species were assigned, it was possible to identify transitions reaching the $(40^{\pm}, 0)$ and $(30^{\pm}, 2)$ states of the $H_2{}^{34}S$ and even of the $H_2{}^{33}S$ isotopomers which were present in natural abundance (4.22% and 0.78%, respectively) in the sample. The observed energy levels of the $H_2{}^{33}S$ and $H_2{}^{34}S$ vibrational states are listed in Tables 5–7, respectively. The rotational and Δ_k centrifugal distortion constants for the vibrational states of $H_2{}^{34}S$ and $H_2{}^{33}S$ were estimated from the corresponding $H_2{}^{32}S$ parameters using simple isotopic relations [9], while the vibrational term value, E_v, parameters were estimated using Eq. (4) of [9]. All higher order parameters as well as the coupling constants were simply fixed to the main isotopomer values. This procedure seems to be very accurate as only 11 parameters were needed to be refined to reproduce 175 observed energy levels of the $H_2{}^{34}S$ isotope within $0.0068\,cm^{-1}$ while 3 parameters were varied to fit 27 energy levels of the $H_2{}^{33}S$ isotope with an rms deviation of $0.010\,cm^{-1}$. The corresponding sets of rotational parameters are included in Table 4.

4. Intensity considerations

The approximate relative intensity values were derived for each absorption line from the peak depth values measured by ICLAS. By using the stronger lines observed in the FT spectrum, the ICLAS intensities were normalized to obtain absolute intensity values. Taking into account the precision of the normalization procedure and possible saturation of the strongest lines, we estimate the experimental accuracy of our measured intensities to 25–30% on average with possible errors up to 100% for the weakest lines. The transition moment parameters were obtained by fitting 1183 (including doublets) line intensities (160 transitions for the $(20^-, 4)$ state, 342 for the $(40^-, 0)$, 323 for the $(30^-, 2)$, 170 for the $(30^+, 2)$, and 185 for the $(40^+, 0)$, state). An rms deviation of 18.3% was achieved by varying 25 parameters. The resulting line intensities are included in Supplementary Material attached to the present paper, which lists 1630 observed line positions and intensities with the corresponding rovibrational assignment and calculated intensities. In the case of blended lines, only transitions contributing to the experimental intensity value by more than 8% were, in general, included in the line list. The quality of the spectrum reproduction is exemplified in Figs. 1–3, which show an overview and some specific sections of the spectrum. In particular, the 9832–9846 cm^{-1} spectral region displayed in Fig. 3 shows that the intensity of the extra lines reaching rotational sublevels of the $(11^+, 4)$ dark state are very well reproduced, supporting, the resonance scheme adopted for the effective Hamiltonian. Despite the good overall agreement between the calculated and observed intensities, poorer results were obtained for some strongly perturbed transitions. This is in particular the case for the transitions reaching the $(40^{\pm}, 0)$ [7 2 5] and the $(30^{\pm}, 2)$ [7 4 3] levels which are strongly interacting.

It is interesting to note that the mixing coefficients of the wavefunctions corresponding to the fourfold energy levels clusters of the local mode pair are highly sensitive to the resonance scheme adopted. As a result, the calculated intensity distribution between the components of the local mode pair is rather unstable for transitions reaching fourfold energy levels clusters: according to the interaction scheme, the calculated intensity is transferred between the two components of the $(40^{\pm}, 0)$ LM pair leading to ambiguities in the vibrational assignments. However, the total intensity of the four involved transitions is unchanged. Despite the fact that only doubly degenerate transitions were included into the fit of the dipolar moment parameters, the intensity prediction for very strong fourfold degenerate experimental lines of the $(40^{\pm}, 0)$—(0 0 0) bands is very satisfactory (see the line list). We have some evidence that the intensity redistribution between the components of the $(40^{\pm}, 0)$ LM pair is correctly reproduced by our model: the calculations show that transitions reaching fourfold clustered levels with $J \geqslant 7$ and $K_a = 0, 1$ have noticeably different frequencies and the corresponding experimental center of the (blended) line generally coincides with that calculated for the most intense component. For example, the center of the line at 9689.582 cm^{-1} with an experimental intensity of $1.1 \times 10^{-7}\, cm^{-2}\, atm^{-1}$ is close to the calculated position of the doubly degenerated line $(40^+, 0)$ [15 0 15]–[16 1 16], [15 1 15]–[16 0 16] (9689.583 cm^{-1}) calculated with an intensity of $9.9 \times 10^{-8}\, cm^{-2}\, atm^{-1}$, while the component of the same fourfold cluster—$(40^-, 0)$ [15 0 15]–[16 0 16], [15 1 15]–[16 1 16] is predicted at 9689.595 cm^{-1} with a significantly weaker intensity ($4.8 \times 10^{-8}\, cm^{-2}\, atm^{-1}$). In consequence, the line intensities were used as an important criterion in the choice of the optimal set of resonance parameters between the components of the $(40^{\pm}, 0)$ LM pair. Further refinements of the theoretical modeling of the line intensities would require more accurate intensity measurements.

The integrated band intensities were obtained as the sum of the individual calculated line intensities larger than $2.5 \times 10^{-9}\, cm^{-2}/atm$. They are included in Table 1 where the results of the intensity calculations of [15] are also given for comparison. We emphasize that the integrated intensities estimated for the $(20^+, 4)$ and $(11^+, 4)$ dark states are very approximate. It should be noted also that the *vibrational* band intensities calculated in [15] may, in case of strong rovibrational coupling, significantly differ from our integrated values. However, the integrated band intensities for the 1st and 2nd hexads as well as for the 1st decade of H_2S [14] were found in satisfactory agreement with the results of [15] with maximum deviations of ±100%. Much larger discrepancies are noted in the higher excited spectral region presently considered, especially for the $(30^{\pm}, 2)$—(0 0 0), and $(40^+, 0)$—(0 0 0) bands (see Table 1). Part of this discrepancy may result from different vibrational assignment of absorption lines resulting from the large mixing of the wavefunctions of the clustered levels. In this case, the comparison of the sum of the integrated intensities reaching the two components of the LM pair is probably more meaningful. Still the discrepancies are too considerable to be explained by this reason indicating that the electric dipole moment function of H_2S derived in [15] is not accurate for the highly excited vibrational transitions. The difficulty of intensity calculations from a dipole moment function in H_2S has been previously analyzed as resulting of the dramatic consequences on the calculated intensities of a small change of the potential energy surface [15–18]. In this context, the potential function and the ab initio dipole moment surface calculated by Tyuterev et al. [16,18] will be highly valuable for such intensity calculations.

5. Conclusion

The present investigation of the near infrared spectrum of H_2S illustrates the performances of the ICLAS-VECSEL method. The use of VECSELs as amplification media gives access to the near infrared spectrum with compact, simple diode pumped ICLAS spectrometer.

The detailed analysis of the H_2S spectrum between 9540 and 10 000 cm^{-1} has allowed determining 892 energy levels. This number should be compared to a total number of 4175 levels used as input data in the determination of the potential energy surface of [17]. A complicate interaction system involving seven vibrational states, four of them being evidenced for the first time, has been successfully modeled. A comparison of the vibrational term values included in Table 1 shows a good agreement with the values predicted by the effective Hamiltonian model of [10]. The comparison with the values calculated from the potential function of [16] is also given and shows an excellent agreement for the three isotopomers. The larger deviations (up to 0.9 cm^{-1}) observed for the dark levels of $H_2{}^{32}S$ are probably due to the effective character of the experimental term value which was extrapolated from a fit of very few rotational levels observed through local resonance interaction with bright states.

Acknowledgments

We are indebted to A. Garnache (CEM2, Université de Montpellier) and A. Kachanov (Picarro, Sunnyvale, California) for the development of ICLAS-VECSEL in Grenoble and for providing the VECSEL samples. This work was sponsored by EU (contract SPHERS HPRN-CT-2000-00022) and by a collaborative Convention between CNRS and the Chinese Academy of Science (No. 12491) as well as by a CNRS–RFBR-PICS (Grant 01-05-2002). O. Naumenko acknowledges the financial support from the Russian Foundation for Basic Researches (Grants Nos. 02-03-32512 and 02-07-90139). V.G. Tyuterev (Université de Reims, France) is acknowledged for communicating the unpublished vibrational term values calculated from the potential energy surface of [16].

References

[1] A. Garnache, A.A. Kachanov, F. Stoeckel, R. Planel, Optics Lett. 24 (1999) 826–830.
[2] A. Garnache, A.A. Kachanov, F. Stoeckel, R. Houdré, J. Opt. Soc. Am. B 17 (2000) 1589–1598.
[3] A. Campargue, L. Biennier, A. Garnache, A. Kachanov, D. Romanini, M. Herman, J. Chem. Phys. 111 (1999) 7888–7903.
[4] E. Bertseva, A. Kachanov, A. Campargue, Chem. Phys. Lett. 351 (2002) 18–26.
[5] Y. Ding, E. Bertseva, A. Campargue, J. Mol. Spectrosc. 212 (2002) 219–222.
[6] O. Vaittinnen, L. Biennier, A. Campargue, J.-M. Flaud, L. Halonen, J. Mol. Spectrosc. 184 (1997) 228–289.
[7] J.-M. Flaud, O. Vaittinen, A. Campargue, J. Mol. Spectrosc. 191 (1998) 262–268.
[8] A. Campargue, J.-M. Flaud, J. Mol. Spectrosc. 194 (1999) 43–51.
[9] O. Naumenko, A. Campargue, J. Mol. Spectrosc. 209 (2001) 242–253.
[10] O. Naumenko, A. Campargue, J. Mol. Spectrosc. 210 (2001) 224–232.
[11] A. Bykov, O. Naumenko, M. Smirnov, L. Sinitsa, L.R. Brown, J. Crisp, D. Crisp, Can. J. Phys. 72 (1994) 989–1000.
[12] L.S. Rothman, C.P. Rinsland, A. Goldman, S.T. Massie, D.P. Edwards, J.-M. Flaud, A. Perrin, C. Camy-Peyret, V. Dana, J.Y. Mandin, J. Schroeder, A. McCann, R.R. Gamache, R.B. Wattson, K. Yoshino, K.V. Chance, K.W. Jucks, L.R. Brown, V. Nemtchinov, P. Varanasi, J. Quantum Spectrosc. Radiat. Transfer 60 (1998) 665–710.
[13] J.-M. Flaud, C. Camy-Peyret, J.W.C. Johns, Can. J. Phys. 61 (1983) 1462–1473.
[14] L. Brown, O. Naumenko, E. Polovtseva, L. Sinitsa, in preparation.
[15] J. Senekowitsch, S. Carter, A. Zilch, H.-J. Werner, N.C. Handy, P. Rosmus, J. Chem. Phys. 90 (1989) 783–794.
[16] Vl.G. Tyuterev, S. Tashkun, D.W. Schwenke, Chem. Phys. Lett. 348 (2001) 223–234.
[17] T. Cours, P. Rosmus, Vl.G. Tyuterev, Chem. Phys. Lett. 331 (2000) 317–322.
[18] T. Cours, P. Rosmus, Vl.G. Tyuterev, J. Chem. Phys. 117 (2002) 5192–5209.